PRAMANA — journal of physics

Vol. 82, No. 1
January 2014
pp. 3–14

Imaging unsteady three-dimensional transport phenomena

K MURALIDHAR
Department of Mechanical Engineering, Indian Institute of Technology Kanpur, Kanpur 208 016, India
E-mail: kmurli@iitk.ac.in

DOI: 10.1007/s12043-013-0638-9; ***e*Publication:** 5 January 2014

Abstract. Careful and continuous measurements of flow, heat and mass transfer are required in quite a few contexts. Using appropriate light sources, it is possible to map velocity, temperature, and species concentration over a cross-section and as a function of time. Image formation in optical measurements may rely on scattering of radiation from particles. Alternatively, if the region of interest is transparent, refractive index would be a field variable and beam bending effects can be used to extract information about temperature and concentration of solutes dissolved in liquids. Time-lapsed images of light intensity can be used to determine fluid velocity. Though used originally for flow visualization, optical imaging has now emerged as a powerful tool for quantitative measurements. Optical methods that utilize the dependence of refractive index on concentration and temperature can be configured in many different ways. Three available routes considered are interferometry, schlieren imaging, and shadowgraph. Images recorded in these configurations can be analysed to yield time sequences of three-dimensional distributions of the transported variables. Optical methods are non-intrusive, inertia-free and can image cross-sections of the experimental apparatus. The image data can be jointly analysed with the physical laws governing transport and principles of image formation. Hence, with the experiment suitably carried out, three-dimensional physical domains with unsteady processes can be accommodated. Optical methods promise to breach the holy grail of measurements by extracting unsteady three-dimensional data in applications related to transport phenomena.

Keywords. Optical measurement; fluid flow and transport; refractive index technique; data retrieval; image analysis.

PACS Nos 07.60.–j; 78.20.Ci; 05.60.Cd; 47.85.–g; 42.30.Wb; 02.30.Zz; 42.30.Wb

1. Introduction

Engineering applications involving transport of energy, mass, and momentum are considerable. Optical methods were introduced early on for visualizing transport processes but have now evolved to become powerful tools of quantitative measurement [1–5]. As a result, optical techniques are extensively used for high precision diagnostics and process

monitoring in physical, biological, and engineering sciences. While initial approaches were based on visible light including lasers, optical techniques have expanded to include a much larger spectrum of electromagnetic radiation. The popularity of optical techniques stems from the fact that they are non-intrusive and can perform whole-field measurement with minimal time lag. Yet the demands of measurement are continuously on the increase. Ultimately, one would like to measure unsteady three-dimensional scalar and vector fields under realistic conditions. Other types of measurements include determination of wall fluxes, say, of heat, from wall temperatures and the estimation of material properties on various scales. Optical methods can be stretched to include a wide range of measurements, first by factoring in the physical laws that govern the process in progress and next, by including the principle of image formation itself. These steps help in utilizing incomplete and imperfect visualization for reconstructing a complete scenario of the transport process itself.

Optical methods can be broadly classified as (i) scattering techniques and (ii) transmission techniques [5]. When a beam of light (wavelength λ) falls on a particle of size d, the scattered radiation will show certain changes. These are with respect to intensity, directionality, wavelength, phase, polarization, and other properties of the wave. The property that shows the most pronounced change depends on the ratio of the wavelength and the particle dimension. Broadly speaking, we have the following limits:

$$\text{Ray optics: } \frac{\lambda}{d} \ll 1; \text{ Wave optics: } \frac{\lambda}{d} \sim 1; \text{ Quantum optics: } \frac{\lambda}{d} \gg 1.$$

Methods such as laser Doppler velocimetry (LDV), particle image velocimetry (PIV), and particle tracking velocimetry (PTV) rely on scattering for measurement of fluid velocity [2–6]. Liquid crystal thermography, laser-induced fluorescence, Mie scattering, and coherent anti-Stokes Raman spectroscopy (CARS) are examples that determine temperature and species concentration. Absorption-based measurements can also be classified as scattering. In transmission methods, the medium is taken to be transparent and the measurement is based on changes in refractive index. Interferometry, schlieren imaging, and shadowgraph are notable examples [7–9]. Measurement at fluid–fluid interfaces is enabled when optical imaging is based on reflected light.

Many of the highlights of optical measurements can be brought out by considering examples of transmission-based techniques. These form the bulk of the following discussion.

1.1 *Refractive index techniques*

The basic ideas involved in such measurements in fluids are first introduced. The fluid medium is taken to be transparent to the passage of light. The light intensity distribution and contrast generated depend on changes in refractive index in the region of interest. Optical techniques such as interferometry, schlieren imaging (monochrome and colour), coherent gradient sensing, and shadowgraph are inter-related. Interferometry is limited by beam bending errors that in turn form the foundation of schlieren and shadowgraph techniques. Using multiple wavelength lasers, distribution of several variables can be jointly determined. Apart from being non-intrusive, optical methods of measurement are

known to have specific advantages in terms of spanning a field-of-view and being inertia-free. The ability to record a time sequence of optical images in a computer using CCD cameras and frame grabbers has permitted complex data analysis. In addition, it is possible to enhance image quality by manipulating light intensity values representing the image. When optical images are viewed as projection data of thermal and species concentrations, three-dimensional variation of the field variable is reconstructed by suitable algorithms, for example, tomography [10,11]. The entire approach can be extended to time-dependent applications as well. Taken together, optical measurements show a route forward by which unsteady three-dimensional measurements of velocity, temperature, and species concentration are possible.

In transparent media, the interaction of light with the material is via the refractive index n. The utility of refractive index arises from the fact that, for isotropic transparent media, it is a unique function of material density. Density, in turn, will depend on temperature and species concentration. Hence, inhomogeneities in the refractive index field will carry information related to heat and mass transfer processes. Independently, anisotropic nature of refractive index has been exploited using polarized light in rheology [12].

2. Optical configurations

Optical configurations such as interferometry, schlieren imaging and shadowgraph exploit changes in refractive index with temperature and species concentration [7,8]. The lay-out of each of the three imaging techniques used in the present work is shown in figure 1. For measurements, a continuous wave helium–neon laser (Spectra Physics, 35 mW) can serve as the coherent light source. A monochrome CCD camera (Sony, Model: XC-ST50) of spatial resolution of 768 $\times$ 574 pixels (or better) records the optical images of the convective field. The camera may be interfaced with a personal computer (HCL, 1 GB RAM, 1.5 GHz) through a 12-bit A/D card.

The principle of operation of a Mach–Zehnder interferometer is shown in figure 1a. It has two mirrors and two 50% beam splitters of 150 mm diameter. The mirrors have a 99.9% silver coating and employ a silicon dioxide layer as a protective layer. The interferometer floats on pneumatic legs to isolate the optics from external vibrations. Experiments are carried out in the infinite as well as the wedge fringe settings. In the infinite fringe setting, the optical path difference between the test and the reference beams is initially zero and a bright field of constructive interference is formed. When a density disturbance is introduced in the path of the test beam, it is seen as a set of fringes over which the depth-averaged density is a constant. In the wedge fringe setting, the optics is slightly misaligned to produce a set of straight fringes – horizontal or vertical. When exposed to a thermal or concentration field, the fringes are displaced to an extent depending on the change in temperature or concentration. The fringes in the wedge fringe setting of the interferometer are thus representative of changes in temperature or concentration. Closely related to the arrangement of figure 1a is dual wavelength interferometry [3] for measuring multiple properties and phase shifting interferometry [13] for controlling resolution.

The schlieren system is of the Z-type, as shown in figure 1b. It includes concave mirrors of 1.30 m focal length and 200 mm diameter. Relatively large focal lengths make the

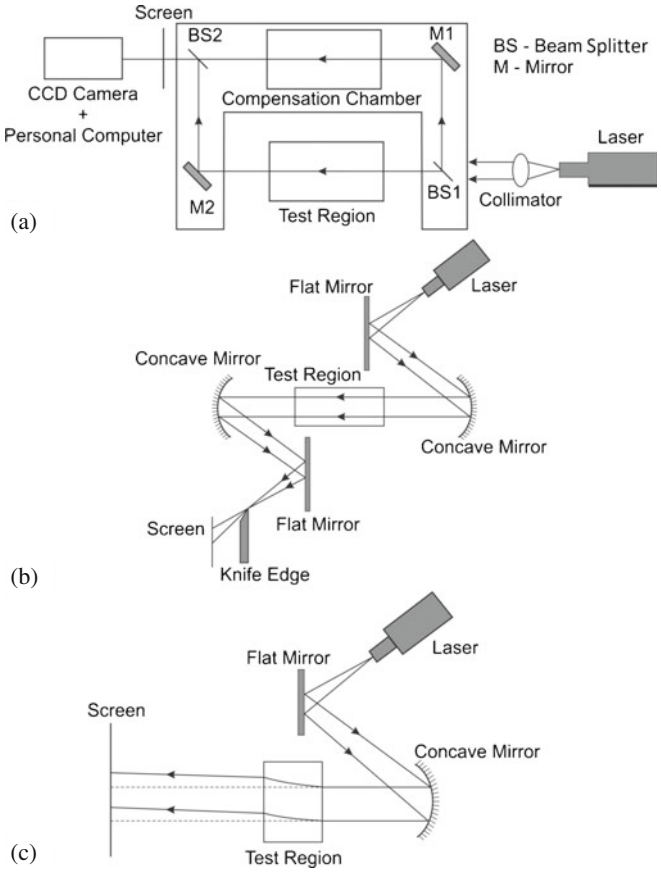

Figure 1. Optical configurations of (**a**) Mach–Zehnder interferometer, (**b**) laser schlieren, and (**c**) shadowgraph.

schlieren technique sensitive to the concentration gradients. The knife-edge is placed at the focal length of the second concave mirror. It is positioned to cut off a part of the light focussed on it, so that in the absence of any optical disturbance, the illumination on the screen is uniformly reduced. The initial intensity values in the experiment are chosen to be less than 20, on a gray scale of 0–255. The knife-edge is set perpendicular to the direction in which the density gradients are to be recorded. In the present study, the gradients are expected to be predominantly in the vertical direction and the knife-edge has been kept horizontal. Further developments in the subject have led to colour schlieren [14] and coherent gradient sensing [15] that improve the appearance of the image formed and simplify analysis.

Shadowgraph images are recorded using the optical components employed in schlieren imaging but without the decollimating optics and the knife-edge (figure 1c). The position of the screen on which the shadowgraph images are displayed plays an important role in data analysis [16–18]. The screen position is chosen so as to improve the image contrast, while extracting the dominant features of the flow field. In both schlieren imaging and

shadowgraph, beam refraction from regions of high concentration gradients can interfere with those passing through one of nearly constant concentration. This factor is taken into account while fixing the camera position. The initial intensity distribution in shadowgraph experiments is the Gaussian variation of the laser itself, corrected for its passage through the pin hole of the spatial filter. The helium–neon laser can be replaced by a white light source and the knife-edge by a gray scale or colour filter in a schlieren arrangement.

In contrast to interferometry where information is localized at the fringes, schlieren and shadowgraph images carry information related to the local temperature or concentration in the form of an intensity distribution. The advantage here is that data are available at the pixel level of the camera. Drawbacks include the errors due to superimposed noise associated with scattering and the possibility of device saturation. The first factor is taken to be less significant because the field variable is obtained by integrating the intensity distribution, an operation that tends to smooth noisy profiles. The second factor is circumvented by reducing the laser intensity using a neutral density filter.

3. Data analysis

Refractive index techniques depend on the fact that for a transparent material, refractive index n and density ρ have a unique relationship of the form [2,5]

$$\frac{n^2-1}{\rho\left(n^2+2\right)} = \text{constant}. \tag{1}$$

Equation (1) is called the Lorentz–Lorenz formula. In gases, $n \sim 1$ and it simplifies to

$$\frac{n-1}{\rho} = \text{constant}. \tag{2}$$

Hence, in gases, the derivative $\mathrm{d}n/\mathrm{d}\rho$ is a constant. In liquids, the derivative is nearly constant if the bulk changes in density are small. For moderate changes in temperature (say, up to around 10°C in air), density and temperature T are linearly related. It follows that $\mathrm{d}n/\mathrm{d}T$ is constant and changes in temperature will simultaneously manifest as changes in refractive index. This result carries over to mass transfer problems as well, where density changes occur from a solutal concentration field. In this formulation, pressure changes can be duly accommodated.

The dependence of refractive index on wavelength λ is often given by the Cauchy's formula [19]

$$n_\lambda = A + \frac{B}{\lambda^2} + \frac{C}{\lambda^4}. \tag{2a}$$

The dependence is stronger in liquids and solids when compared to gases. The first two terms may be adequate in most applications. The Lorentz–Lorenz formula is a special case of a more general dependence function of refractive index on density. The general form is written in the form of a virial expansion in the dependent variables ρ, T, and C as follows:

$$\frac{n^2-1}{n^2+2} = a_0 + a_1\rho + a_2T + a_3C. \tag{2b}$$

The individual dependence on temperature and concentration (apart from density) is usually small for most media. Hence, it is sufficient to generalize this equation as

$$\frac{n^2-1}{n^2+2} = a_0 + a_1\rho. \tag{2c}$$

The correction has negligible effect in gases. In liquids, the derivative $\mathrm{d}n/\mathrm{d}\rho$ may be altered by 5–10% when the second term is included in calculations.

The governing equations for each of the optical methods are summarized below.

Interferometry: Consider the passage of a laser through a test section of length L in the viewing direction. For a light source of wavelength λ the change in concentration/temperature required per fringe shift ΔC_ε (or ΔT_ε) in the infinite fringe setting is given as [2,5,7,8]

$$\Delta C_\varepsilon = \frac{\lambda/L}{\mathrm{d}n/\mathrm{d}C}; \qquad \Delta T_\varepsilon = \frac{\lambda/L}{\mathrm{d}n/\mathrm{d}T}. \tag{3}$$

The fringe positions are to be determined from interferogram analysis. In the wedge fringe setting, it can be shown that the fringe displacement from the initial position is proportional to the change in concentration with respect to the portion of the solution where the fringes are undisturbed. These results hold under the approximation that the light beam travels in a straight line and beam deflection and displacement effects are small.

Schlieren imaging: Image formation in a schlieren system is due to deflection of the light beam in a variable refractive index field towards regions that have a higher refractive index. In order to recover quantitative information from a schlieren image, one has to determine the cumulative angle of refraction of the light beam emerging from the growth chamber as a function of position in the cross-sectional x–y plane normal to the light beam, whose direction of propagation is along the z-coordinate. Using principles of ray optics, the total angular deflection δ can be expressed as [9]

$$\delta = \frac{1}{n_\mathrm{a}} \int_0^L n \frac{\partial \ln(n)}{\partial y} \mathrm{d}z. \tag{4}$$

Here n is the refractive index at any point in the physical domain and n_a refers to the ambient. The change in the intensity field ΔI relative to the background intensity distribution I_k can now be related to the refractive index field directly as

$$\frac{\Delta I}{I_\mathrm{k}} = \frac{f}{a_\mathrm{k} \times n_\mathrm{a}} \int_0^L \frac{\partial n}{\partial y} \mathrm{d}z. \tag{5}$$

Here n_a, the refractive index of the ambient is practically unity, a_k is the size of the focal spot at the knife-edge, and f is the focal length of the de-collimating mirror (or lens). This equation shows that the schlieren technique records the integrated gradient of refractive index over the path of the light beam. In terms of the ray-averaged refractive index, the governing equation for the schlieren process can be derived as

$$\frac{\Delta I}{I_\mathrm{k}} = \frac{f}{a_\mathrm{k} \times n_\mathrm{a}} \frac{\partial n}{\partial y} \times L. \tag{6}$$

The above equation requires the approximation that changes in the light intensity occur due to beam deflection, rather than its physical displacement. The contribution of refraction of light at the confining optical windows needs to be accounted for.

Shadowgraph: The shadowgraph arrangement depends on the change in the light intensity arising from beam displacement from its original path. Shadowgraph analysis requires tracing the path of individual rays through the fluid region. When subjected to linear approximations that include small displacement of the light ray, a second-order partial differential equation can be derived for the refractive index field with respect to the intensity contrast in the shadowgraph image. With D as the distance of the screen from the exit plane of the experimental apparatus and Δ as the Laplace operator in the x–y plane, this equation is expressed as [16]

$$\frac{\Delta I}{I_{\mathrm{k}}} = L \times D\Delta \left\{\ln n(x, y)\right\}. \tag{7}$$

Here, I_{k} is the initial intensity distribution and ΔI is the change in intensity at a pixel, the ratio of the two defining contrast. The above equations have to be suitably integrated to determine the refractive index, and hence, the concentration (or temperature) field. Integration of the Poisson equation can be performed by a numerical technique, say the method of finite differences. When the approximations involved in the derivation of the above equations do not apply, optical techniques can be used for flow visualization alone [1].

3.1 *Inverse techniques*

Data retrieval from optical images can be augmented when the principle behind image formation is brought into analysis. However, this approach can lead to considerably higher analytical complexity. Specifically, information regarding the field variables such as temperature can be obtained by solving 'inverse' problems as exemplified here. Consider a medium with refractive index n that depends on all the three space coordinates, namely $n = n(x, y, z)$. In the context of a shadowgraph measurement, we are interested in tracing the path of light rays as they pass through this medium. Starting with the knowledge of the angle and the point of incidence of the ray at the entrance plane, we would like to know the location of the exit point on the exit window, and the curvature of the emergent ray [16–18].

Let the ray be incident at point $P_{\mathrm{i}}(x_{\mathrm{i}}, y_{\mathrm{i}}, z_{\mathrm{i}})$ and the exit point be $P_{\mathrm{e}}(x_{\mathrm{e}}, y_{\mathrm{e}}, z_{\mathrm{e}})$. According to Fermat's principle the optical path length traversed by the light beam between these two points has to be an extremum. If the geometric path length is L, then the optical path length is the product of the geometric path length with the refractive index of the medium. Thus

$$\delta\left(\int_{P_{\mathrm{i}}}^{P_{\mathrm{e}}} n\,(x, y, z)\,\mathrm{d}s\right) = 0. \tag{8}$$

Parametrizing the light path by a coordinate z, the above condition can be represented in terms of two functions $x(z)$ and $y(z)$, and the equation can be rewritten as

$$\delta\left(\int_{z_i}^{z_e} n\,(x, y, z)\,\sqrt{x'^2 + y'^2 + 1}\;\,\mathrm{d}z\right) = 0, \tag{8a}$$

where primes denote differentiation with respect to z. Application of the variational principle to the above equation yields two coupled Euler–Lagrange equations, that can be written in the form of the following differential equations for $x(z)$ and $y(z)$:

$$x''(z) = \frac{1}{n}\left(1 + x'^2 + y'^2\right)\left(\frac{\partial n}{\partial x} - x'\frac{\partial n}{\partial z}\right), \tag{9}$$

$$y''(z) = \frac{1}{n}\left(1 + x'^2 + y'^2\right)\left(\frac{\partial n}{\partial y} - y'\frac{\partial n}{\partial z}\right). \tag{10}$$

The four constants of integration required to solve these equations come from the boundary conditions at the entry plane of the chamber. These are the coordinates $x_i = x(z_i)$, $y_i = y(z_i)$ of the entry point z_i and the local derivatives $x'_i = x'(z_i)$, $y'_i = y'(z_i)$. The solution of the above equation yields the two orthogonal components of the deflection of the ray at the exit plane, and also its slope. When a large number of rays are traced, the intensity distribution on the exit plane and the screen can be determined.

Equations (9) and (10) can be solved for the coordinates if the three-dimensional refractive index distribution is known. This is the 'direct' problem and involves integrating a nonlinear system of ordinary differential equations. Much harder is the calculation of the refractive index function $n(x, y, z)$ from the knowledge of the ray coordinates on the exit plane. This is an inverse problem and specialized tools are needed for analysis.

3.2 *Tomography*

Much of the optical imaging is performed in planes while the measured variable itself is posed in three dimensions. Projecting a three-dimensional field onto a plane is a direct problem; the reverse which is common to optical imaging is an inverse problem. Tomography is an analytical technique available for reconstruction of the three-dimensional data from two-dimensional projections [5,10,11].

Physical systems of interest have three-dimensional variation of flow, temperature, and species concentration within the apparatus. When interferometry, schlieren imaging or shadowgraph imaging is employed, one obtains a depth-averaged view of the three-dimensional variation (eqs. (3)–(7)). The image data is often called path integral or projection of the thermal (or concentration) field. Tomography is a procedure for recovering the three-dimensional information of the field variable from a collection of projections. The projection data are recorded at various angles by turning the experimental apparatus or the light beam, specifically the source–detector axis. Algorithms such as convolution back-projection (CBP) and algebraic reconstruction (ART) have been developed in this context [5,7,10,11]. Tomographic algorithms are known to be sensitive to noise in projection data. Issues such as sensitivity and the impact of having limited data need to be considered [20].

In general, tomography is a technique for extracting spatial and temporal information about process parameters by using multiple sensors mounted around the process of interest. The sensor system is chosen dependening on which parameters or characteristics to be imaged. For example, electromagnetic radiations (such as X-rays and γ-rays) are sensitive to the changes in densities in the medium of interest, whereas capacitance sensors are sensitive to the dielectric constant of the object. Irrespective of the medium under study,

the sensor signals are amplified, possibly also filtered and multiplexed, digitized and sent into a computer in which a cross-section of the measured parameter is reconstructed and displayed.

Tomographic algorithms can be classified into [11]: (a) transform, (b) series expansion, and (c) optimization methods. Transform methods generally require a large number of projections for a meaningful answer. In optical measurements, projections can be recorded either by rotating the experimental set-up or the source detector combination. Rotating the source–detector combination is particularly difficult and more so with the kind of optical configurations employed for crystal growth studies due to stringent requirement of alignment. With the first option, it is not possible to record a large number of projections, partly owing to inconvenience and partly due to time and cost. Hence, as a rule, a large number of projections cannot be acquired and one must look for algorithms that converge with just a few projections. Limited-view tomography is best accomplished using the series expansion method. As limited-view tomography does not have a unique solution, the convergence of these iterative algorithms is expected to be sensitive to the initial guess of the field that starts the iterations. Optimization-based algorithms are known to be independent of initial guess, but the choice of the optimization function plays an important role in the result obtained. Depending upon the mathematical definition used, the entropy extremization route may yield good results, while the energy minimization principle may be suitable in other applications.

Ideally, one needs to record information simultaneously from all the view angles. This demands multiple source–detector combinations and necessitates stringent alignment requirements, making the experimental configuration relatively expensive. Often, a finite amount of time elapses while moving from one view angle to the other. Hence, the projection data recorded are asynchronous in time particularly if the temporal changes in the concentration gradients are faster than the speed at which the projection data is recorded from different view angles. This difficulty can be circumvented if the projection data from all view angles are correlated. A method such as proper orthogonal decomposition (POD) is useful as it decouples the spatial and temporal components of the measured time-dependent data [20–22]. The spatial modes, in turn, are ordered across all projections, thus facilitating three-dimensional reconstruction over the entire physical domain.

4. Applications

Evolution of thermal convection in an air-filled differentially heated eccentric annulus is shown in figure 2 as interferograms. A time sequence of schlieren images in the wake of a heated oscillating circular cylinder is shown in figure 3. Mixed convection patterns around a KDP crystal growing from a supersaturated aqueous solution are shown in figure 4; see [23] for a discussion on optical methods in crystal growth. The undisturbed image of the screen and the starting transient of a helium jet in the ambient are shown in figure 5.

Future developments in refractive index methods are likely to see the following trends:

(1) Combined measurements using, say, schlieren imaging (in high-gradient regions) and interferometry (in low-gradient regions)

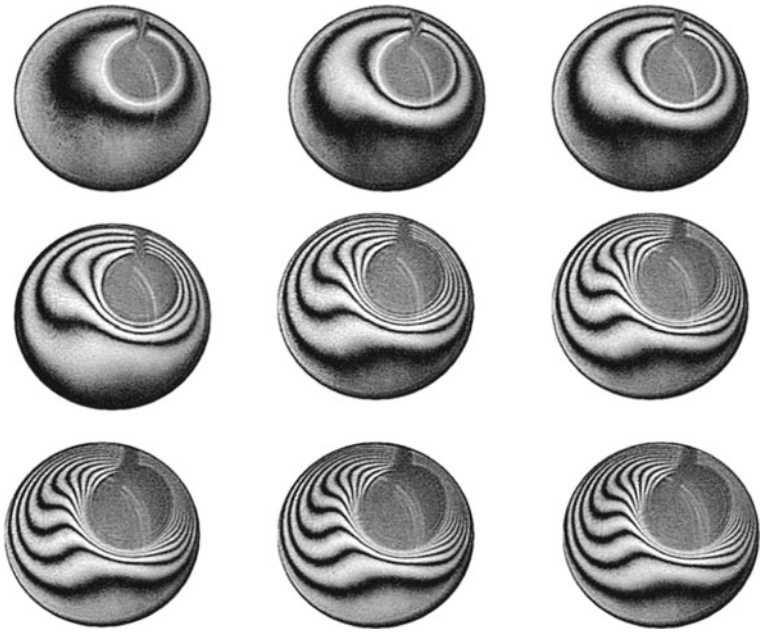

Figure 2. Imaging of thermal convection in an eccentric air-filled annulus at selected time instants using a Mach–Zehnder interferometer in the infinite fringe setting.

(2) Usage of multiple wavelengths of the laser including white light sources
(3) Extension to measurement with other radiation sources
(4) Superior analytical tools for image analysis
(5) Surface topography measurements
(6) Utility in field-scale applications, satellite-level imaging of natural phenomena
(7) Imaging of transport phenomena at microscales, in MEMS, for example
(8) Bulk property measurement such as thermal diffusivity in complex fluids and biological solutions.

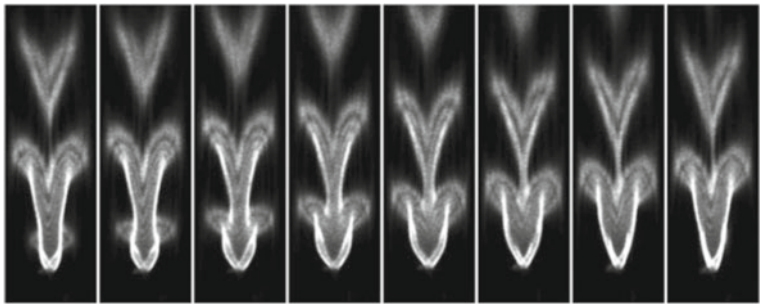

Figure 3. Instantaneous schlieren images in the wake of a strongly heated circular cylinder oscillating at 1.5 times the natural frequency of vortex shedding. Main flow is in the vertically upward direction.

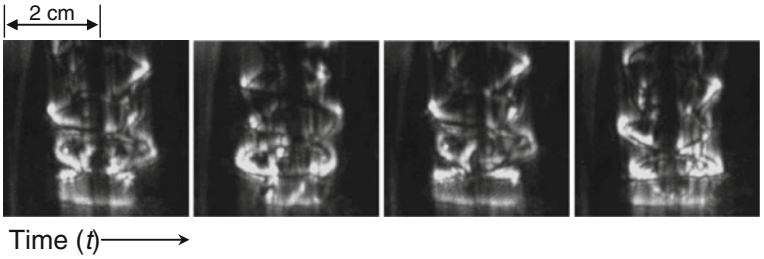

Figure 4. Schlieren images of the time-dependent convective field around a KDP crystal growing from its aqueous solution at four different time instants. Bright regions are zones of high concentration gradients. The dark region away from the crystal shows the undisturbed supersaturated solution.

5. Closure

Images of fluid flow, heat transfer, and species transport can be recorded using radiation-based techniques. Among the options available, the one based on refractive index changes in a transparent medium is discussed. The measurement is over a cross-section and follows transients without delay. The recorded data can be analysed to recover additional details such as three dimensionality and unsteadiness as well as surface-level fluxes. Such an approach will require knowledge of the natural laws that govern transport as well as principles of image formation from radiation sources.

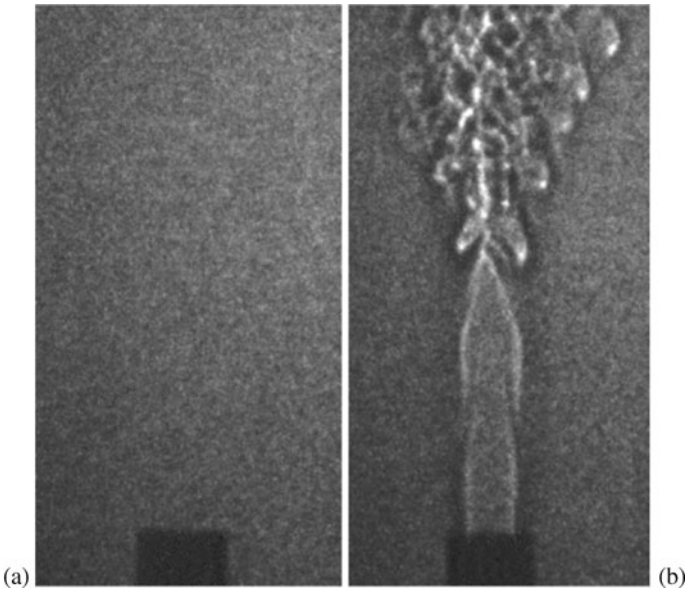

Figure 5. Undisturbed screen (**a**) and light intensity perturbations created in a shadowgraph arrangement (**b**) when a helium jet is released in the normal atmosphere.

References

[1] W F Merzkirch, *Flow visualization*, 2nd edn (Academic Press, New York, 1987)
[2] R Goldstein (ed.), *Fluid mechanics measurements*, 2nd edn (Taylor and Francis, New York, 1996)
[3] M Lehner and D Mewes, *Applied optical measurements* (Springer-Verlag, Berlin, 1999)
[4] W Lauterborn and A Vogel, *Ann. Rev. Fluid Mech.* **16**, 223 (1984)
[5] F Mayinger (ed.), *Optical measurements: Techniques and applications* (Springer-Verlag, Berlin, 1994)
[6] C Tropea, A L Yarin and J F Foss (eds), *Springer handbook of experimental fluid mechanics* (Springer, Berlin, 2007)
[7] K Muralidhar, *Ann. Rev. Heat Transfer* **12**, 265 (2001)
[8] P K Panigrahi and K Muralidhar, *Schlieren and shadowgraph methods in heat and mass transfer* (Springer Briefs in Thermal Engineering and Applied Science, New York, USA, August, 2012); *Imaging heat and mass transfer processes - Visualization and analysis* (Springer Briefs in Thermal Engineering and Applied Science, New York, USA, October 2012)
[9] G S Settles, *Schlieren and shadowgraph techniques* (Springer, Berlin, 2001)
[10] G T Herman, *Image reconstruction from projections* (Academic Press, New York, 1986)
[11] F Natterer, *The mathematics of computerized tomography* (John Wiley, New York, 1986)
[12] G Schmidt, A I Nakatani and C C Tan, *Rheol. Acta* **41**, 45 (2002)
[13] J Min, B Yao, P Gao, R Guo, J Zheng and T Ye, *Appl. Opt.* **49**, 6612 (2010)
[14] K Al-Ammar, A K Agrawal, S R Gollahalli and D Griffin, *Exp. Fluids* **25**, 89 (1998)
[15] B Atcheson, W Heidrich and I Ihrke, *Exp. Fluids* **46**, 467 (2009)
[16] W Schopf, J C Patterson and A M H Brooker, *Exp. Fluids* **21**, 331 (1996)
[17] S Rasenat, G Hartung, B L Winkler and I Rehberg, *Exp. Fluids* **7**, 412 (1989)
[18] R W Lewis, R E Teets, J A Sell and T A Seder, *Appl. Opt.* **26(17)**, 3695 (1987)
[19] P Schiebener, J Straub, J M H L Sengers and J S Gallagher, *J. Phys. Chem. Ref. Data* **19(3)** (1990)
[20] A Srivastava, K Muralidhar and P K Panigrahi, *Prog. Cryst. Growth Charact. Mater.* **58**, 209 (2012)
[21] L Sirovich, *Quart. Appl. Math.* **45(3)**, 561 (1987)
[22] A Srivastava, D Singh and K Muralidhar, *J. Crystal Growth* **311**, 1166 (2009)
[23] S Verma and P J Schlicta, *Prog. Crys. Growth Charact. Mater.* **54**, 1 (2008)